

Room- and Low-Temperature Crystallographic Study of the Ambient Pressure Organic Superconductor (Bisethylene dithiotetrathiofulvalene)₄Hg_{2.89}Br₈

Ruiming Li, Vaclav Petricek,[†] Guangdi Yang,[‡] and Philip Coppens*

Department of Chemistry, Natural Sciences and Mathematics Complex,
State University of New York at Buffalo, Buffalo, New York 14260-3000

Michael Naughton

Department of Physics, Fronczak Hall, State University of New York at Buffalo,
Buffalo, New York 14260-1500

Received September 25, 1997. Revised Manuscript Received March 10, 1998

(BEDT-TTF)₄Hg_{2.89}Br₈ (BEDT-TTF = bisethylene dithiotetrathiofulvalene) is an ambient pressure low-temperature superconductor ($T_c = 4.3\text{K}$) with an incommensurate two-sublattice structure. It crystallizes in orthorhombic and monoclinic modifications. Only the monoclinic phase becomes superconducting on cooling, as confirmed in this study. Its Hg sublattice undergoes a transition when the temperature is reduced, during which the Hg columns gradually shift in a direction parallel to the column axis. Since the symmetry is lowered, twinning occurs, but the structure of the conducting layers of BEDT-TTF molecules is little affected. The structures at room temperature and 40K are analyzed using four-dimensional superspace group theory.

Introduction

(BEDT-TTF)₄Hg_{2.89}Br₈ (BEDT-TTF = bisethylene dithiotetrathiofulvalene) is a solid with unusual physical properties that consists of two interpenetrating incommensurate lattices.^{1,2} The incommensurability of the BEDT-TTF molecules and Br atoms in one substructure and the Hg atoms in a second substructure necessarily leads to nonintegral stoichiometry. (BEDT-TTF)₄Hg_{2.89}Br₈ crystallizes in both monoclinic and orthorhombic phases, which have similar cell dimensions and related structures. The monoclinic modification has been described as an ambient pressure superconductor, with a midpoint of the transition at about $\approx 4.3\text{K}$, and vanishing resistance at $\approx 3.7\text{K}$.² The conductivity of (BEDT-TTF)₄Hg_{2.89}Br₈ is highly anisotropic and much larger in the plane of the sheets of BEDT-TTF molecules than perpendicular to the sheets. Unlike other BEDT-TTF salts, the critical temperature (T_c) of the monoclinic phase increases with pressure to reach a maximum of $\approx 6.7\text{K}$ at $\sim 3.5\text{kbar}$. The decrease of T_c above 10 kbar has been attributed to a possible change in structure under the influence of pressure.³ A third phase with orthorhombic symmetry has been analyzed by Li⁴ and may be identical to one of the phases mentioned, but

not further described, in the literature.² A strong isotope effect was found on deuteration; κ -(BEDT-TTF)₄Hg₃Br₈ has a commensurate structure containing Hg–Hg dimers rather than Hg columns and is not an ambient pressure superconductor, though superconductivity occurs on application of small pressures.⁵ The Cl analogue, (BEDT-TTF)₄Hg_{2.78}Cl₈, has an incommensurate structure and is a superconductor with $T_c = 1.8\text{K}$ at 12 kbar.

We describe here the four-dimensional structure (i.e., the structure of both sublattices and their modulations) of the monoclinic phase and its gradual transformation on cooling to a phase in which the second sublattice is triclinic. To use the four-dimensional space groups in their standard setting, the incommensurate direction has been labeled as the c -axis. Thus the Hg columns are directed along c , and the conducting plane parallel to the sheets of BEDT-TTF molecules is labeled as the bc -plane.

Experimental Section

Electrocrystallization. The procedure described by Lyubovskaya et al. for preparation of the monoclinic phase of (BEDT-TTF)₄Hg_{2.89}Br₈ uses a constant current of $0.5\ \mu\text{A}$, applied to a solution containing 2 mM BEDT-TTF, 15 mM Bu₄NHBr₃, and 1 mM HgBr₂ in trichloroethane (TCE) at a temperature of $40\ ^\circ\text{C}$.⁶ Attempts to duplicate this procedure were unsuccessful, but good-quality, black, shiny plates were obtained by electrocrystallization at room temperature in a

[†] Present address: Institute of Physics, Academy of Sciences of the Czech Republic, Cukrovarnicka 10, Praha 6-Stresovice, Czech Republic.

[‡] Present address: Department of Chemistry, Jilin University, P. R. China.

(1) Lyubovskii, R. B.; Lyubovskaya, R. N.; Dyachenko, O. A. *J. Phys. I Fr.* **1996**, *6*, 1609.

(2) Lyubovskaya, R. N.; Zhilyaeva, E. I.; Pesotskii, S. P.; Lyubovskii, R. B.; Atovmyan, L. O.; Dyachenko, O. A.; Takhirov, T. G. *Pis'ma v ZhETF* **1987**, *46*, 149.

(3) Schirber, J. E.; Overmyer, D. L.; Venturini, E. L.; Wang, H. H.; Carlson, K. D.; Kwok, W. K.; Kleinjan, S.; Williams, J. M. *Physica C* **1989**, *161*, 412.

(4) Li, R. Thesis, State University of New York at Buffalo, Buffalo, NY, 1994.

(5) Lyubovskii, R. B.; Lyubovskaya, R. N.; Luppov, A. E.; Dyachenko, O. A.; Gritsenko, V. V.; Makova, M. K.; Merzhanov, V. A. *J. Phys. I Fr.* **1993**, *3*, 2411.

(6) Lyubovskaya, R. N.; Aldoshina, M. Z.; Goldenberg, L. M.; Zhilyaeva, E. I. *Synth. Met.* **1991**, *41–43*, 2143.

Table 1. Crystallographic Information

	monoclinic phase		triclinic phase	orthorhombic phase
	this study		this study	ref 4
space group	RT		40 K	RT
$D_{\text{calc}}(\text{g cm}^{-3})$	$P.C2/c-11(0,0,\gamma)$		$P.C-1:-1$	$P.Pmcr:11-1(0,0,\gamma)$
$\mu(\text{cm}^{-1})$	2.520		2.515	2.508
M_r	261.27		261.83	
$F(000)$	2755.72		2755.72	2755.72
	2288		2288	2288
	monoclinic phase		triclinic phase	orthorhombic phase
	(a) Sublattice I			
	this study	ref 2 ^a	this study	ref 4
	RT	RT	40 K	RT
$a(\text{Å})$	38.610(3)	38.582(2)	38.413(8)	37.21(1)
$b(\text{Å})$	8.717(1)	8.706(2)	8.597(3)	8.718(2)
$c(\text{Å})$	11.222(1)	11.219(3)	10.963(4)	11.273(3)
$\alpha(\text{deg})$			90	90.003(7)
$\beta(\text{deg})$	74.058(7)	74.07(4)	74.746(3)	89.997(1)
$\gamma(\text{deg})$			90	90.027(3)
$V(\text{Å}^3)$	3631.4(8)	3623.6(13)	3492.8(19)	3657(2)
Z	2	2	2	2
	(b) Sublattice II and Ratio of Sublattice Volumes			
	this study	ref 2	this study	ref 4
	RT	RT	40 K	RT
space group	$P.C2/m:-1s$		$P.C-1$	$P.Pmmr:1s-1$
$a(\text{Å})$	37.543(3)	37.141(7)	37.84(2)	37.26(5)
$b(\text{Å})$	8.717(1)	8.706(2)	8.672(8)	8.719(2)
$c(\text{Å})$	3.893(1)	3.877(1)	3.81(1)	3.872(4)
$\alpha(\text{deg})$			96.97(2)	90.019(7)
$\beta(\text{deg})$	81.39(1)	87.30(4)	79.020(4)	90.021(2)
$\gamma(\text{deg})$			91.38(1)	89.975(4)
$V(\text{Å}^3)$	1259.7(4)	1252.2(5)	1218(3)	1258(3)
Z	2	2	2	2
$V(\text{I})/V(\text{II})$	2.883(1)	2.894(2)	2.868(7)	2.907(7)

^a Transformed from $I2/a$ to $C2/c$.

U-shaped cell with Pt electrodes, using a tetrahydrofuran (THF) solution of 2 mM BEDT-TTF, 1 mM (*n*-Bu)₄NHgBr₃, and 50 mM HgBr₂ and a current of 0.5 μ A applied for 48 h. On the other hand, using a TCE solution of 1.5 mM BEDT-TTF and 22.7 mM Bu₄NHgBr₃ and a constant current of 0.4 μ A gave black, shiny plates consisting mainly of the orthorhombic phase. Subsequent diffraction analysis showed that the crystals grown in this manner usually contain both monoclinic and orthorhombic domains, with a common orientation of the *a*- and *b*-axes.

Preliminary Diffraction Measurements. Room-temperature oscillation and Weissenberg photographs of both phases show patterns typical for a two-sublattice crystal, with extra layers due to the second lattice. On *c*-axis oscillation photographs the $l \neq 0$ reflections of the Hg sublattice are superimposed on diffuse streaks extended perpendicular to the oscillation axis, indicating a lack of full registry between the heights of different Hg columns.

Though composite crystals are aperiodic in at least one dimension, the symmetry can be recovered by use of the superspace group description, in which (for the four-dimensional case) an extra dimension is introduced perpendicular to three-dimensional space.⁷ For the *monoclinic* phase, the $hklm$ reflections obey the condition $h + k = 2n$, while the $h0lm$ reflections show the condition $l = 2n$, indicating the superspace group $P.C2/c-11(00\gamma)$ or $P.Cc:1(00\gamma)$. The former choice is confirmed by the structure analysis. Since there are four (BEDT-TTF)₄Hg_{2.89}Br₈ formula units in the cell, the BEDT-TTF molecules are in general positions. The embedded space group of the Hg lattice is $P.C2/m:-1s$. As there are two mercury atoms in the second subcell, they are located at special positions with $2/m$ symmetry. For the *orthorhombic* phase, the reflection conditions are $hk0m$, $h + k = 2n$ and $h0lm$, $l =$

$2n$, corresponding to the space group $P.Pmcr:11-1(00\gamma)$. The embedded space group for the Hg lattice is $P.Pmmr:1s-1(00\gamma)$.

Table 1 summarizes the space groups and lattice parameters of the various phases, as determined in the present study and reported by Li⁴ and Lyubovskaya et al.^{1,2} In the current presentation the *c*-axis is chosen as the direction common to both sublattices. The cell of Lyubovskaya et al. has been transformed to this convention by interchange of the *a*- and *c*-axes. The ratios of the volumes of the two sublattices, which imply the stoichiometry, are listed in the last column of Table 1. The ratio varies from 2.868(7) for the 40 K phase to 2.883(1) for the room-temperature monoclinic phase and to 2.907(7) for the orthorhombic phase. As the errors may be somewhat underestimated, none of the values gives convincing evidence for a deviation from the earlier used stoichiometry (BEDT-TTF)₄Hg_{2.89}Br₈, which is retained in the current paper.

Conductivity Measurements. Electrical conductivity measurements were made on both types of crystals. The resistance of a sample of the orthorhombic modification is shown in Figure 1a, measured via a dc four-probe method with gold paste contacts to 10 μ m diameter gold wires. On the initial cool down (trace 1), metal-like behavior is observed from room temperature to about 150 K, where a broad minimum in $R(T)$ is seen. At lower temperatures, nonmetallic, semiconducting-like behavior occurs, with a distinguishable slope change at 20 K. The warming curve (trace 2) retraces this cool down. A current of 1 μ A was used here, corresponding to $\sim 10^{-2}$ A/cm² current density. Upon immediately recooling the sample with 0.1 μ A current (trace 3), the sample remains metallic down to ~ 15 K before the upturn, signifying a transition to semiconducting behavior. These data show an obvious and strong dependence on electrical current, though stress-induced changes in conductivity may play a role as well.

The monoclinic crystals generally remained metallic down to the lowest temperatures measured. However, due to the more fragile nature of these crystals, this behavior was

(7) Janner, A.; Janssen, T. *Acta Crystallogr.* **1980**, *A36*, 408. Van Smaalen, S. J. *Phys. Condens. Matter* **1989**, *1*, 2791.

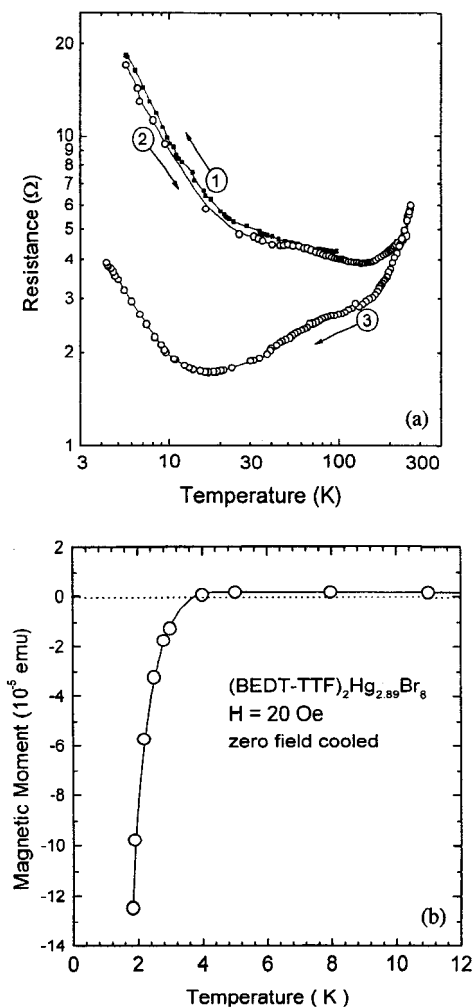


Figure 1. Results of physical measurements: (a) resistance of the orthorhombic phase and (b) magnetic moment of the monoclinic phase.

invariably interrupted by microcracks, which led to sharp jumps in the resistance. Nonetheless, the superconducting transition was verified by both resistivity and susceptibility. The magnetization plot in Figure 1b shows that the onset of superconductivity occurs at about 4 K, consistent with the literature.³

Structural Change on Cooling

For examination of the behavior of the superconducting monoclinic phase on cooling, a crystal was cooled to 40 K in a diffractometer-mounted cryostat. Lowering of the symmetry was evident from *c*-axis oscillation diagrams, recorded with imaging plates, which revealed the presence of two equivalent, triclinic, Hg sublattices but no splitting of the reflections due to sublattice I. Oscillation pictures taken at 260, 150, 100, and 40 K showed a gradually increasing deviation of the α angle from 90°. The lattice parameters for the low-temperature phase are included in Table 1. The change in the α angle from 90° to 97° on cooling corresponds to a relative shift of two Hg columns separated by the *b* lattice spacing, with a magnitude of 1.06 Å along the *c* direction (Figure 2). At the same time, as the β angles of the two sublattices differ less at low temperature, the shift, relative to the A sublattice, of two Hg columns separated by the large *a* cell dimension is reduced from

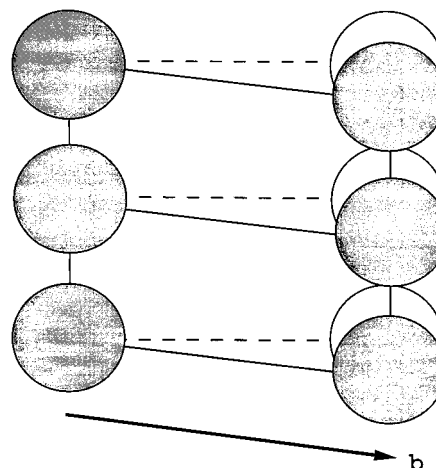


Figure 2. Illustration of the phase transformation of the Hg lattice on cooling. Filled circles, Hg atoms at 40 K; open circles, Hg atoms at room temperature. At $y = 0$ both positions are identical. Since a lowering of the symmetry is involved, in half of the domains the Hg atoms shift in the opposite direction, leading to twinning.

Table 2. Data Collection and Refinement

	monoclinic phase				
	room temperature	40 K			
crystal size	diamond shaped plate; same as rt ^a 0.525 × 0.08 × 0.05 mm; forms {1,1,1}; large face, {1,0,0}				
diffractometer	CAD4/scint. counter	Huber/imaging plates (oscillation method)			
scan method	$\theta/2\theta$				
oscillation method	6° oscillations				
radiation	Cu K α , $\lambda =$ 1.5418 Å	Mo K α , $\lambda =$ 0.7110 Å			
sin θ/λ range	0–0.56 Å ⁻¹	0.08–1.01 Å ⁻¹			
no. of refl					
before averaging	8670	11587			
after averaging, $I > 3\sigma(I)$	3253	4380			
transmission factors	0.046–0.367	0.20–0.59			
Final Agreement Factors (%)					
	all	<i>hk0l</i>	<i>hk0m</i>	<i>hk00</i>	<i>hklm</i> , $l \neq 0, m = 1$
<i>R</i>					
rt	6.35	5.91	8.02	2.51	15.16
40 K	6.32	5.39	10.41	3.80	15.30
<i>R_w</i>					
rt	7.92	9.31	9.71	6.21	16.21
40 K	7.52	6.37	10.45	4.47	15.64

^a Room temperature.

4.92 Å at room temperature to 2.92 Å at 40 K. The interaction between the Hg atoms of substructure II and the adjacent Br atoms of substructure I is affected by these shifts and by the change in the displacive modulation amplitudes. The interaction is further analyzed below, using the results of the diffraction analysis.

The Nature of Composite Structures and the Relation between the Two Sublattices

Multi-sublattice, composite crystals are defined by the coexistence of two or more lattices in a single material. In general, the two lattices are incommensurate in at least one-direction, but their relative orientations and

Table 3. Relative Orientation of Two BEDT-TTF Molecules in the Low-Temperature Phase

	rotations (deg) around			translations (Å) along		
	a	a × b	b	a	b	c
molecule 1	0	0	0	-0.00017(10)	-0.0020(4)	-0.0018(4)
molecule 2	0	0	180.25(10)	0.00012(10)	-0.8354(4)	0.5020(4)

positions are restricted by space-fitting requirements.⁸ Since there is a mutual interaction between the two components with different translational repeat, each will be modulated with the period of the lattice of the other component.

In a composite crystal, the two sublattices in real space and the corresponding reciprocal space lattices are related by the "interlattice" matrixes σ and σ^* , defined through the relations

$$\mathbf{A}_{\text{Hg}} = \sigma \mathbf{A}_{(\text{ET}+\text{Br})} \quad (1a)$$

and

$$\mathbf{A}^*_{\text{Hg}} = \sigma^* \mathbf{A}^*_{(\text{ET}+\text{Br})} \quad (1b)$$

where the matrixes \mathbf{A} and \mathbf{A}^* represent the real and reciprocal axial systems respectively, and ET is used as an abbreviation for BEDT-TTF. The matrixes follow directly from the orientation matrixes of the two lattices as determined from diffractometer angles of the Bragg reflections. For the two phases of (BEDT-TTF)₄-Hg_{2.89}Br₈ the matrixes are as follows

monoclinic phase (RT)	orthorhombic phase	
$\sigma = \begin{pmatrix} 1 & 0 & -0.444 \\ 0 & 1 & 0 \\ 0 & 0 & 0.347 \end{pmatrix}$	$\begin{pmatrix} 1 & 0 & 0 \\ 0 & 1 & 0 \\ 0 & 0 & 0.343 \end{pmatrix}$	
$\sigma^* = \begin{pmatrix} 1 & 0 & 0 \\ 0 & 1 & 0 \\ 1.28 & 0 & 2.88 \end{pmatrix}$	$\begin{pmatrix} 1 & 0 & 0 \\ 0 & 1 & 0 \\ 0 & 0 & 2.911 \end{pmatrix}$	(2)

Thus, in both phases the *b* and *c*-axes of the two sublattices are parallel, but with different repeat along the *c*-axes for the two sublattices, while the *a**- and *b**-axes of the two sublattices are identical. The diffraction pattern can therefore be described on a basis of four reciprocal vectors. For the monoclinic phase the fourth vector is given by

$$\mathbf{a}_4^* = 1.28\mathbf{a}_1^* + 2.88\mathbf{a}_3^* \quad (3)$$

as follows from (2).

The main reflections of the BEDT-TTF + Br and Hg sublattices have indices *hk*0 and *hk*0*m*, respectively, the *hk*00 plane being common to both sublattices. A general reflection *hklm*, with the lattice vector $\mathbf{Q} = h\mathbf{a}_1^* + k\mathbf{a}_2^* + l\mathbf{a}_3^* + m\mathbf{a}_4^*$, is an *m*th order satellite of first sublattice as well as an *l*th order satellite of the second sublattice.

Data Collection, Data Reduction, and Determination of the Average Structure. Data collection details are summarized in Table 2. Equivalent reflections were averaged and reduced to structure factors using programs written by Blessing.⁹ Numerical absorption corrections were applied.

Table 4. Fractional Coordinates

	x	y	z
Composite Part 1			
(first line, room temperature; second line, 40 K)			
Br1	0.44193(4)	0.9209(2)	0.3019(2)
	0.4427(1)	0.8992(4)	0.3014(5)
Br1'	0.4410(1)	-0.9032(4)	0.8090(4)
Br2	0.50035(4)	0.7521(2)	0.5402(2)
	0.4994(1)	0.7541(5)	0.5547(3)
Br2'	0.4999(1)	-0.7515(5)	1.0540(4)
S1	0.774003(0)	0.505341(0)	0.00000(0)
	0.774254(0)	0.509648(0)	-0.00200(0)
S2	0.75473(8)	0.2845(4)	0.2064(3)
	0.7549(1)	0.2833(4)	0.2059(3)
S3	0.85017(9)	0.5286(4)	-0.0038(3)
	0.85058(9)	0.5339(4)	-0.0051(4)
S4	0.82672(9)	0.2667(4)	0.2438(3)
	0.8272(1)	0.2633(4)	0.2462(4)
S5	0.67197(8)	0.3044(4)	0.2060(3)
	0.67213(9)	0.3010(4)	0.1981(4)
S6	0.69022(8)	0.5217(4)	0.0002(3)
	0.69106(9)	0.5271(4)	-0.0093(4)
S7	0.59334(9)	0.3209(5)	0.2412(4)
	0.59380(9)	0.3043(4)	0.2172(6)
S8	0.61585(9)	0.5931(4)	0.0047(4)
	0.6169(1)	0.5898(4)	-0.0180(6)
C1	0.7401(2)	0.401(1)	0.1029(8)
	0.7405(2)	0.400(1)	0.1011(9)
C2	0.8081(2)	0.449(1)	0.0679(8)
	0.8087(2)	0.451(1)	0.0664(9)
C3	0.7993(2)	0.349(1)	0.1602(9)
	0.7998(2)	0.349(1)	0.1611(9)
C4	0.8752(3)	0.471(1)	0.100(1)
	0.8759(2)	0.480(1)	0.107(1)
C5	0.8701(3)	0.312(1)	0.144(1)
	0.8711(3)	0.311(1)	0.144(1)
C6	0.7052(2)	0.407(1)	0.1006(8)
	0.7055(2)	0.408(1)	0.0947(9)
C7	0.6441(2)	0.490(1)	0.0686(9)
	0.6451(2)	0.489(1)	0.053(1)
C8	0.6359(3)	0.388(1)	0.162(1)
	0.6363(2)	0.379(1)	0.147(1)
C9	0.5727(3)	0.511(1)	0.074(1)
	0.5730(3)	0.509(1)	0.052(1)
C10	0.5652(3)	0.465(2)	0.202(1)
	0.5667(3)	0.468(1)	0.191(1)
H1C4	0.8700(0)	0.5428(0)	0.1680(0)
	0.8680(0)	0.5395(0)	0.1872(0)
H2C4	0.9008(0)	0.4871(0)	0.0560(0)
	0.9027(0)	0.4964(0)	0.0696(0)
H1C5	0.8873(0)	0.2970(0)	0.1900(0)
	0.8914(0)	0.2864(0)	0.1824(0)
H2C5	0.8751(0)	0.2510(0)	0.0750(0)
	0.8761(0)	0.2526(0)	0.0594(0)
H1C9	0.5549(0)	0.5719(0)	0.0580(0)
	0.5527(0)	0.5811(0)	0.0457(0)
H2C9	0.5724(0)	0.4117(0)	0.0200(0)
	0.5690(0)	0.4069(0)	0.0086(0)
H1C10	0.5399(0)	0.4274(0)	0.2300(0)
	0.5398(0)	0.4461(0)	0.2241(0)
H2C10	0.5657(0)	0.5555(0)	0.2490(0)
	0.5720(0)	0.5621(0)	0.2233(0)
Composite Part 2			
(first line, room temperature; second line, 40 K)			
Hg	0.0	0.5	0.5
	0.0	0.5	0.5

The average structure of the BEDT-TTF/Br sublattice was solved by direct methods with programs from the

(8) Coppens, P. *Acta Crystallogr.* **1995**, *B51*, 402.

Table 5. Modulation Amplitudes (Å) (first line, room temperature; second line, 40 K)

(a) Atomic Amplitudes				
atoms	wave	U_x	U_y	U_z
Hg ^a	sin(2 πx_4)	0 0.00008(8)	-0.0313(2) -0.0385(1)	0 -0.012(1)
	sin(4 πx_4)	-0.00025(7) -0.00113(4)	0 0.0052(3)	-0.011(2) 0.0130(8)
	sin(6 πx_4)	0 0.00102(9)	0.0093(2) 0.0111(2)	0 0.072(1)
	sin(8 πx_4)	-0.00008(8) -0.00048(5)	0 -0.0069(4)	0.027(1) 0.0147(7)
	sin(2 πx_4)	0.0024(1) 0.0015(2)	0.0108(5) 0.0075(6)	-0.0153(5) -0.0324(6)
Br1	cos(2 πx_4)	0.0035(1) 0.0055(2)	0.0110(6) 0.0068(7)	0.0081(5) -0.0089(8)
	sin(4 πx_4)	-0.0007(3) -0.0007(3)	-0.004(2) 0.001(2)	0.000(1) 0.000(1)
	cos(4 πx_4)	-0.0007(3) -0.0014(2)	0.001(2) 0.0004(5)	0.000(1) -0.0114(6)
Br2	sin(2 πx_4)	-0.0014(2) 0.0037(2)	0.0004(5) -0.0004(9)	-0.0114(6) -0.0171(7)
	cos(2 πx_4)	-0.0003(2) 0.0006(1)	0.0281(5) 0.0366(7)	0.0039(6) -0.0001(7)
	sin(4 πx_4)	-0.0024(4) -0.0006(5)	-0.006(1) 0.002(1)	0.0011(9) 0.002(2)
	cos(4 πx_4)	-0.0006(5)	0.002(1)	0.002(2)
Br1'	40 K only			
	sin(2 πx_4)	0.0046(2)	-0.0090(7)	-0.0145(7)
Br2'	cos(2 πx_4)	0.0045(2)	-0.0098(7)	0.0112(7)
	sin(2 πx_4)	-0.0021(2)	-0.0252(7)	-0.0087(8)
	cos(2 πx_4)	0.0006(1)	-0.0164(8)	0.0268(5)

(b) BEDT-TTF Rigid Body Rotational and Translational Displacements (deg and Å)

modulation wave	rotations around			translations along		
	a	a × b	b	a	b	c
Room Temperature						
sin(x ₄)	1.45(13)	-0.18(8)	0.63(5)	0.022(4)	-0.022(3)	0.017(4)
cos(x ₄)	0.01(13)	0.21(7)	-0.03(5)	0.026(4)	0.072(3)	-0.004(5)
Low Temperature						
molecule 1						
sin(x ₄)	-1.3(2)	0.09(11)	-0.49(9)	0.050(6)	-0.014(5)	0.054(8)
cos(x ₄)	1.0(2)	-0.29(10)	0.89(8)	0.131(5)	-0.027(5)	0.007(6)
molecule 2						
sin(x ₄)	-1.8(2)	-0.59(8)	-0.85(10)	-0.017(6)	-0.029(5)	-0.068(7)
cos(x ₄)	0.4(2)	-0.31(9)	0.05(12)	-0.049(6)	-0.018(5)	-0.014(8)

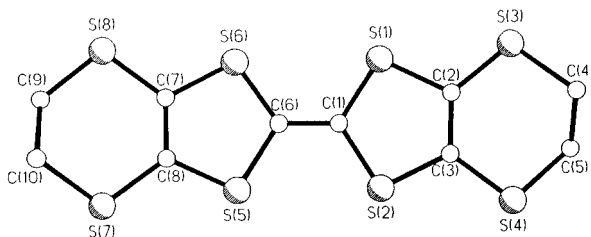
^a Cosine terms not symmetry-allowed.

Figure 3. Molecular drawing showing the numbering of the atoms.

Enraf-Nonius VAX-SDP 3.0 package,¹⁰ and refined by the program package LINEX84.¹¹ Scattering factors (including anomalous contributions) were taken from the International Tables for X-ray Crystallography.¹²

The composite structure was refined by programs JANA93 and JANA96.¹³ The function minimized was $\sum[w(|F_{\text{obs}}| - k|F_{\text{cal}}|)]$, where $w = 1/\sigma^2(F)$, $\sigma(F) = \sigma(F^2)/2F$, and $\sigma(F^2) = [\sigma^2_{\text{counting}} + (0.0004F^4)]^{1/2}$. As the Hg lattice reflections are superimposed over diffuse streaks, only the strongest reflections with a peak intensity several times that of the diffuse streaks were included in the refinement. True satellite reflections (defined as reflections with $l \neq 0$, $m \neq 0$) could only be measured with $m = 1$. Because part of the Hg scattering is into

the diffuse streaks, separate scale factors were used for the $m = 0$ and $m \neq 0$ reflections. The positions of H atoms were calculated and included in the structure factor calculation.

For the low-temperature structure the resolved reflections of both twin components were included in the refinement, using the procedure developed by van Smaalen and Petricek,¹⁴ according to which in the twinned four-dimensional case five indices (h , k , l , m , n) are used to describe the complete diffraction pattern. Reflections which were not resolved in the twinned low-temperature diffraction pattern were omitted. This reduced the number of available data, and required a judicious choice of the variables to be refined. As the unit cell of sublattice I is not distorted in the transition,

(9) Blessing, R. H. *Cryst. Rev.* **1987**, 1, 3.

(10) Enraf-Nonius. VAX-SDP Structure Determination Package, Version 3.0; Enraf-Nonius, Delft, The Netherlands, 1985.

(11) LINEX84; Chemistry Department, State University of New York at Buffalo, USA, 1984.

(12) *International Table for X-ray Crystallography*; Kynoch Press: Birmingham, 1974; Vol. IV (present distribution, Kluwer Academic Publishers: Dordrecht).(13) Petricek, V. *Programs for Modulated and Composite Crystal*; Institute of Physics: Praha, Czech Republic, 1993, 1996. Petricek, V.; Dusek, M. to be published.(14) van Smaalen, S.; Petricek, V. *Acta Crystallogr.* **1992**, A48, 610.

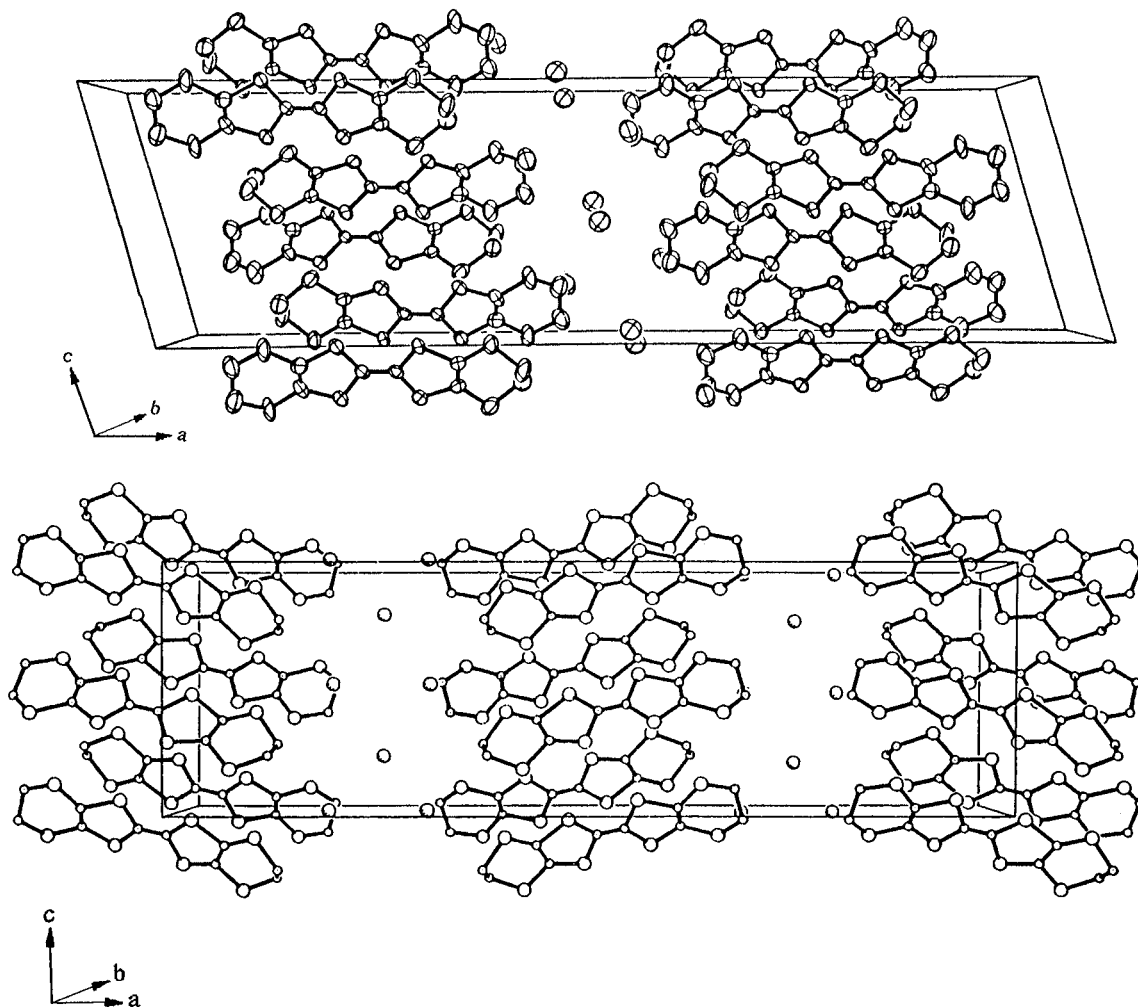


Figure 4. (a) Packing diagram of the monoclinic phase viewed along the *b*-direction. The Hg atoms of sublattice II are omitted. The Hg columns are directed along *c* at 0, 1/2, *z* and 1/2, 0, *z*. (b) As in Figure 4a, for the orthorhombic phase. The Hg columns are directed along *c* at 1/4, 3/4, *z* and 3/4, 3/4, *z*.

the two BEDT-TTF molecules in the asymmetric unit of space group $P\bar{1}$, which are related by the 2-fold screw axis parallel to *b* in the room-temperature structure, were constrained to be identical, but parameters describing their relative orientation were refined. The angle of rotation around the *b*-axis refined to $180.25(10)^\circ$, while the *b*-axis translation was 0.5020(4) (Table 3), indicating that the relationship between the two molecules in the monoclinic phase is retained on cooling. In the low-temperature analysis all atoms except Hg were assigned an isotropic temperature parameter, as the thermal motion was very small. To reduce correlation between parameters, the temperature parameters of Br atoms related by symmetry in the room-temperature monoclinic phase were constrained to be identical in the low-temperature refinement. Table 4 lists the positional parameters for both BEDT-TTF/Br and /Hg substructures. The anisotropic thermal parameters and the bond distances and bond angles in the BEDT-TTF molecule are listed in Tables S1 and S2, respectively, of the Supporting Information.

Modulation Analysis. The displacive modulations result from the mutual interaction between the substructures and are an essential part of any description of a composite structure. In the harmonic analysis of the displacive modulations, the atomic displacements

are described by an expansion of sine and cosine waves multiplied by vectorial amplitudes:

$$\mathbf{u}_\nu = \sum_n \{ \mathbf{U}_{\sin}^{n,\nu} \sin(2\pi n \mathbf{q} \cdot \mathbf{g}_\nu) + \mathbf{U}_{\cos}^{n,\nu} \cos(2\pi n \mathbf{q} \cdot \mathbf{g}_\nu) \} \quad (4)$$

where $\mathbf{U}^{n,\nu}$ is the amplitude vector for atom ν of the wave with wave vector $n\mathbf{q}$, \mathbf{q} is the fundamental modulation vector, and \mathbf{g}_ν is the phase reference point, which may be the position of atom ν or, in the case of a molecule being displaced as a rigid body (the BEDT-TTF molecules are treated in this way in the current analysis), the center of mass of the molecule. The truncation of the series is determined by the necessity to limit the number of variable parameters, and by examination of the convergence of the series; higher harmonics which were found to have nonsignificant amplitudes were omitted in subsequent cycles. Symmetry restrictions described elsewhere were applied.¹⁵ It was found that the modulation of the Hg atom required harmonics up to and including the fourth-order functions, while the Br atom modulation could be adequately described by one and two harmonics for the low- and room-temper-

(15) Petricek, V.; Coppens, P. *Acta Crystallogr.* **1988**, *A44*, 1051.

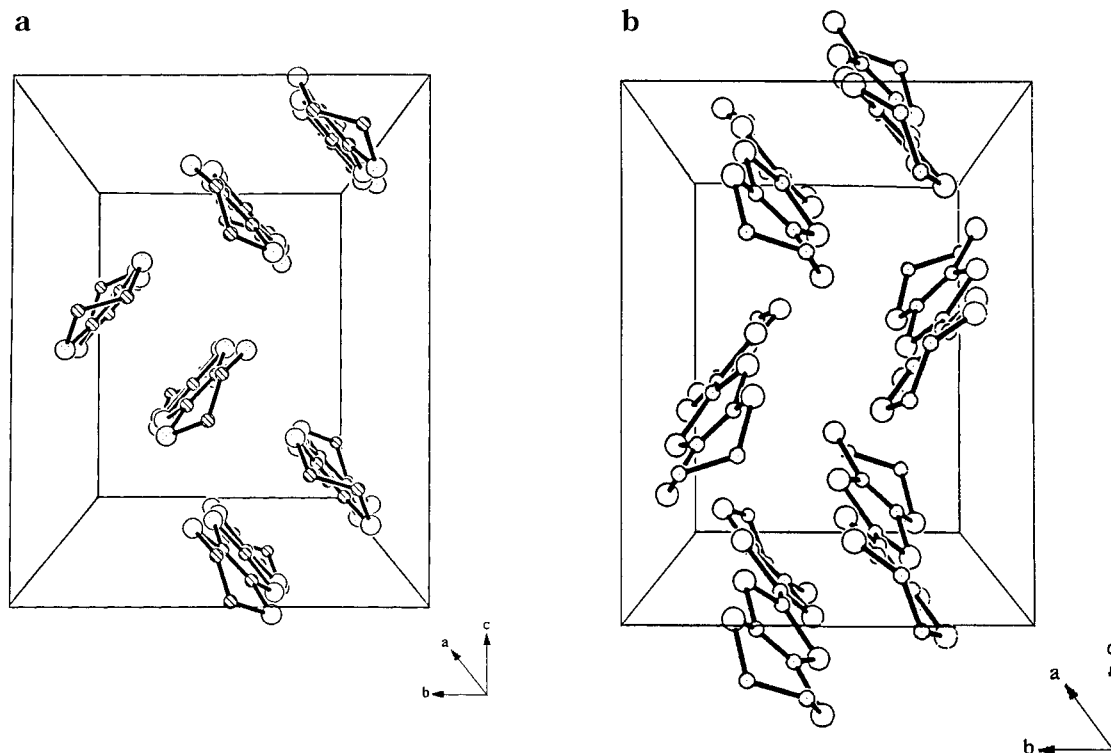


Figure 5. (a) Packing of the BEDT-TTF molecules within one ab -sheet, monoclinic phase viewed along the a -direction. (b) As in Figure 5a, for the orthorhombic phase.

ature structures, respectively. The positional modulation parameters are summarized in Table 5, while the modulation of the temperature parameters is given in Table S3 of the Supporting Information. A drawing of the molecule at low temperature, specifying the numbering of the atoms, is shown in Figure 3.

Results and Discussion

In both room temperature phases, the unit cell of sublattice I contains eight crystallographically equivalent BEDT-TTF molecules and 16 bromine atoms. The relative positions of the origins of the two sublattices follows from the common $hk0$ reflections. Views along the a - and b -directions are given in Figures 4 and 5, respectively, and compared with the corresponding figures for the orthorhombic phase.⁴ The b -axis views show the BEDT-TTF long molecular axes to be approximately aligned with the a -axis direction in both cases, though the packing in the two phases differs significantly in detail. The a -axis view shows stacks of parallel molecules along the b -axis, adjacent molecules in a stack being shifted along both a and c . The molecules in adjacent stacks within an ab -sheet are rotated by about 90° around the c -axis in both phases.

In terms of the classification of ET molecules by Williams et al.,¹⁶ the intrastack packing mode of the BEDT-TTF molecules is described by the a - and b -modes, and the interstack arrangement is described by the w -mode. The bromine atoms are interspersed between the ab -sheets, and are in contact with the

terminal ethylene groups of the BEDT-TTF molecules and with the Hg atoms.

The modulation and thermal parameters of the Hg atom deserve special attention. At room temperature, the modulation along the z -coordinate is not very strong (maximal displacement, 0.15 \AA), but the temperature parameter of the Hg atoms, U_{33} , is unusually large and strongly modulated. This indicates that the mean-square displacements along the z -direction are different in different cells depending on the variation of the interaction with Br atoms of the first subsystem. At low temperature, the modulations of the mean-square displacements are insignificant, but the modulational amplitude of displacement along the z -direction (the z -component of \mathbf{U} in expression 4) is larger.

The x_1x_3 and x_2x_3 sections of the four-dimensional synthesis based on the $hklm$ reflections, containing the Hg atoms, are shown in Figure 6. The Hg atoms are indicated by the dotted strings. The x_1x_3 section shows the Hg modulation in the a -direction, i.e., toward the BEDT-TTF sheets, to be smaller, as is also evident from the modulation amplitudes listed in Table 5.

The interaction between Hg and Br is put on a quantitative basis by mapping all Hg–Br distances in the crystal and calculating the valence sums as a function of the position along the Hg chain. This can be done by making use of the fact that in the four-dimensional description of three-dimensional physical space, the periodicity that is absent in three-dimensional space is recovered. By plotting the distance as a function of the fourth-dimension coordinate, t , all Hg–Br distances that exist anywhere in the aperiodic crystal are represented. Such plots are shown, with and without modulation, for both the room- and low-temperature phases, in Figure 7. It is clear that the mod-

(16) Williams, J. M.; Wang, H. H.; Emge, T. J.; Geiser, U.; Beno, M. A. J.; Whangbo, M. H. *Prog. Inorg. Chem.* **1987**, *35*, 51.

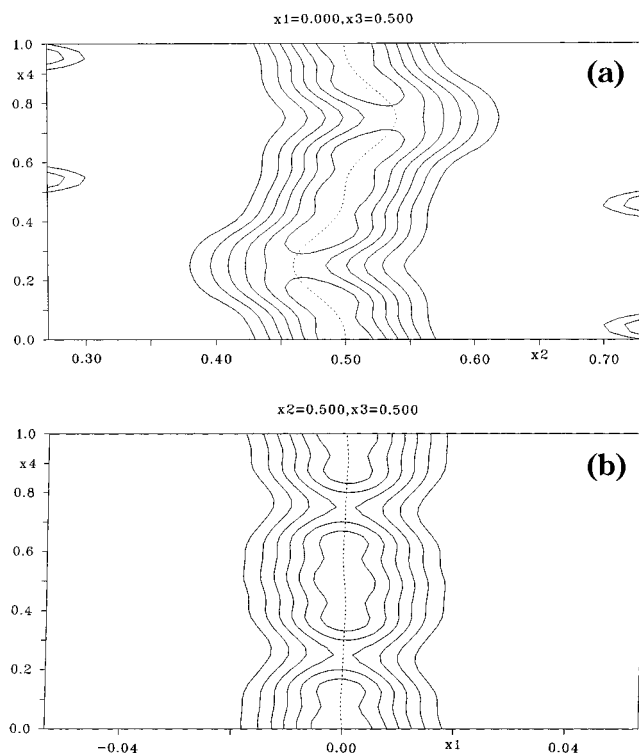


Figure 6. The x_1x_3 and x_2x_3 sections containing the Hg atoms of the four-dimensional Fourier map based on all reflections. Since x_3 is the internal coordinate of sublattice II, the Hg atoms occur as strings, indicating their displacement from the average position in different unit cells.

ulation has the effect of eliminating Hg–Br distances shorter than 2.4 Å, while some longer distances are shortened. The plots show that the modulation is driven by the necessity of avoiding repulsions between very close Hg and Br atoms in the hypothetical nonmodulated structure. The valence sums of Brown,¹⁷ defined as

$$V_i = \sum_j \exp\left(\frac{r_{0,ij} - r_{ij}}{B}\right) \quad (5)$$

with $B = 0.37$, $r_{0,Hg,Br}$ equal to 2.4 Å, and r_{ij} values equal to the observed Hg···Br distances at each value of t , are shown in Figure 8. Though some fluctuations occur, the average valence of the Hg atoms is much more uniform as a result of the modulation, with an average value slightly above 2.2.

For both temperatures average intermolecular S···S distances, which are shorter than the sum of the van der Waals radii (3.6 Å) at 40 K, are listed in Table 6. For the low-temperature phase, those of molecule A are listed, the corresponding average values for molecule B being very similar. The S···S distances generally contract considerably on cooling. Thus, intermolecular transfer integrals and therefore the band structure will be affected, suggesting one of the causes of the strong dependence of the physical properties on temperature. The effect of the modulation on these S···S distances is not as pronounced as its effect on the inter-substructure atomic distances. A representative example of the

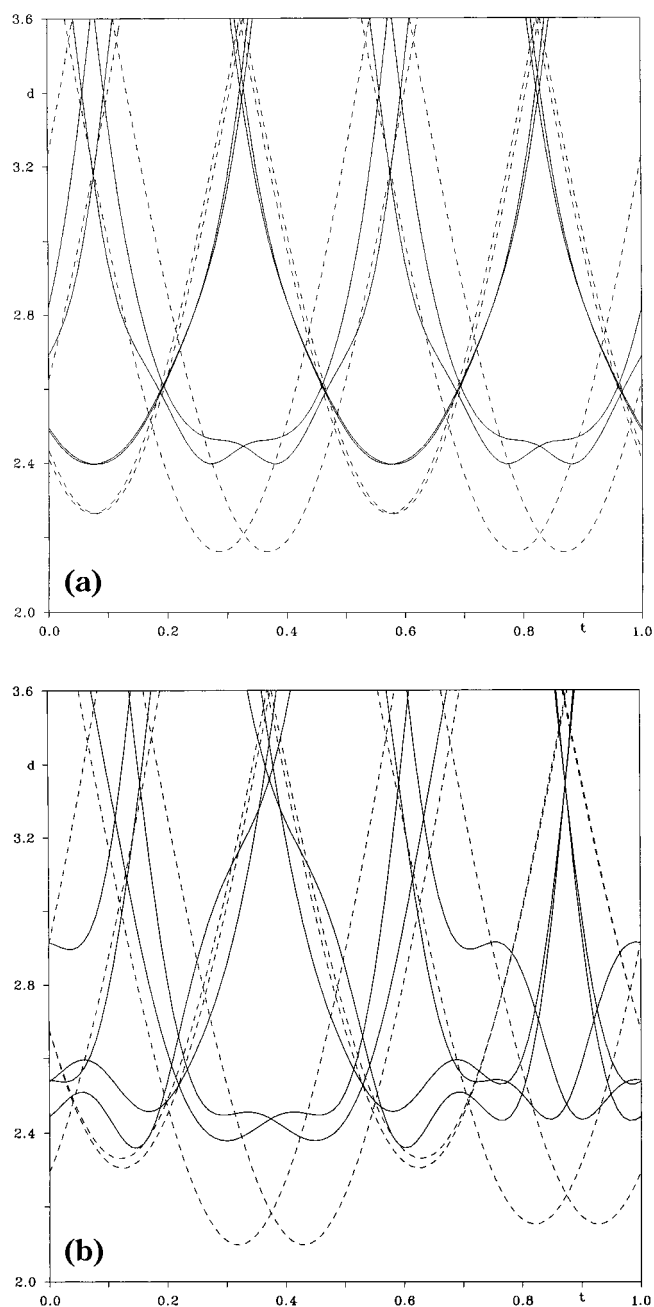


Figure 7. Hg–Br distances as a function of the four-dimensional coordinate t with (full lines) and without (broken lines) the occurrence of the modulation: (a) room temperature, (b) low temperature. Vertical axis in Å.

t -dependence of the S–S distances is given in Figure 9.

Conclusions

The observed phase transition on cooling affects the relative positions of the Hg columns. Its effect on the physical properties of the solids may be minor, as the incommensurability of the two substructures leads to an almost continuous distribution of the relative heights of the Hg and Br atoms along the column axis. The strong dependence of the intermolecular S···S distances on temperature is more likely to affect the transport properties on cooling. A band structure calculation including the modulation is required to analyze the effect of the contraction on the density of states near

(17) Brown, I. D.; Altermatt, D. *Acta Crystallogr.* **1985**, B41, 244.

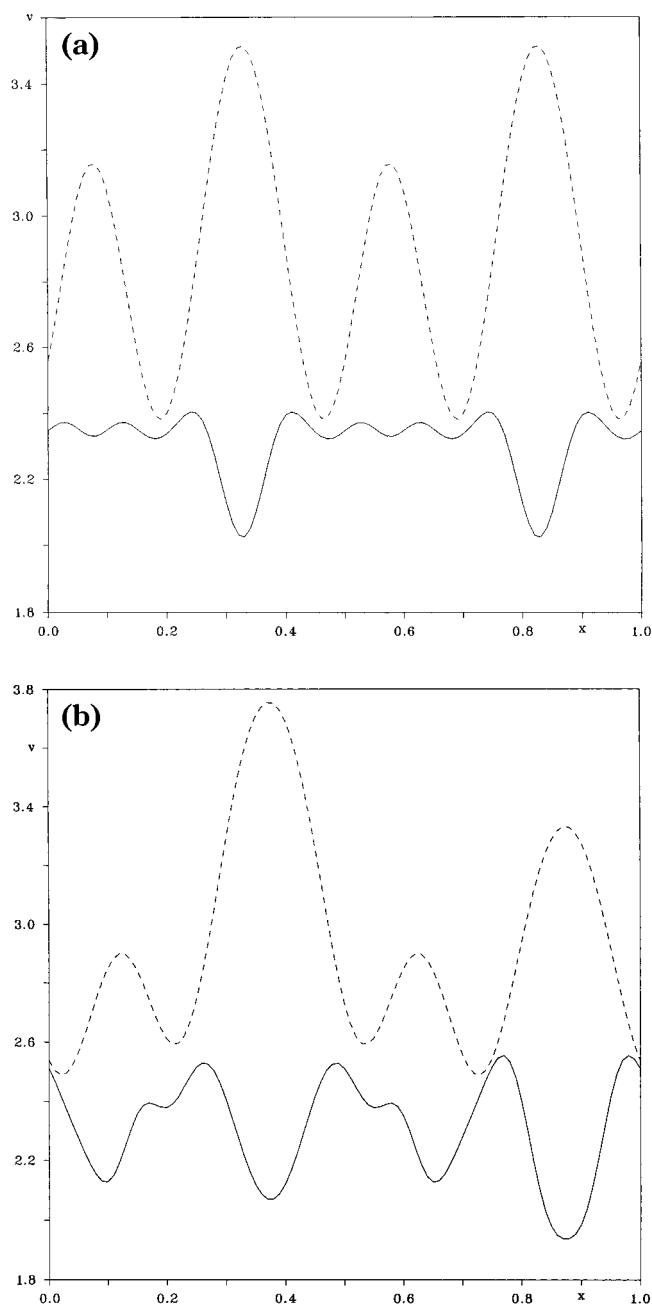


Figure 8. Valence sums for the Hg atom as a function of the four-dimensional coordinate t with (full lines) and without (broken lines) the occurrence of the modulation: (a) room temperature, (b) low temperature.

the Fermi level. The reported conductivity behavior as a function of pressure suggests that additional structural changes may occur on application of pressure. A

Table 6. Average Intermolecular S...S Distances (Å) at Room and Low Temperatures^a

		symmetry code of second atom	room temp	40 K
S1	S4	$x, 1 + y, -1 + z$	3.64	3.55
S3	S8	$3/2 - x, 3/2 - y, -z$	3.55	3.55
	S4	$x, 1 + y, -1 + z$	3.67	3.52
S4	S1	$x, 1 + y, z$	3.64	3.52
	S3	$x, 1 + y, z$	3.67	3.57
	S6	$3/2 - x, -1/2 - y, 1 - z$	3.50	3.42
S5	S8	$x, 1 + y, z$	3.57	3.45
S6	S4	$3/2 - x, 1/2 - y, 1 - z$	3.50	3.48
S7	S8	$x, 1 + y, z$	3.39	3.44
S8	S3	$3/2 - x, 3/2 - y, -z$	3.55	3.55
	S5	$x, 1 + y, -1 + z$	3.57	3.38
	S7	$x, 1 + y, -1 + z$	3.39	3.31

^a Only distances that are shorter than 3.6 Å at 40 K are listed.

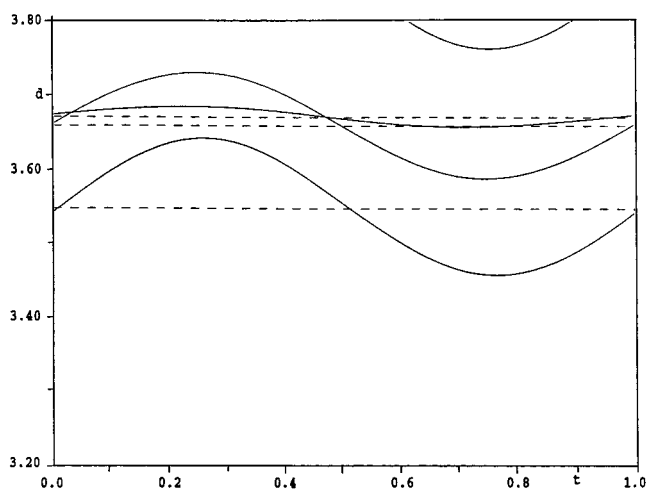


Figure 9. Example of the dependence of the intermolecular S...S distances on the modulation. Distances to atom S1 at low temperature. Full lines, with the modulation. Vertical axis in Å.

low-temperature analysis at 10–12 kbar would be a logical extension of the current study.

Acknowledgment. Support by the National Science Foundation (CHE9317770 and CHE9615586) is gratefully acknowledged. The research of V.P. has been made possible by Grant 202/96/0085 from the Grant Agency of the Czech Republic.

Supporting Information Available: Tables of temperature parameters, bond lengths and angles, and Hg temperature factor modulation parameters (3 pages). Ordering information is given on any current masthead page.

CM9706457